ELSEVIER

Journal of Structural Geology 28 (2006) 1808–1820

JOURNAL OF STRUCTURAL GEOLOGY

www.elsevier.com/locate/jsg

# Regional and local tectonics at Erta Ale caldera, Afar (Ethiopia)

Valerio Acocella*

*Dipartimento di Scienze Geologiche, Università Roma Tre, Largo S.L. Murialdo 1, 00146 Rome, Italy*

Received 15 December 2005; received in revised form 5 June 2006; accepted 23 June 2006
Available online 8 September 2006

**Abstract**

Erta Ale volcano lies along the on-shore Red Sea Rift (northern Afar, Ethiopia), separating the Nubia and Danakil plates. Erta Ale has a NNW–SSE elongated caldera, with a subvertical rim scarp, hosting a lava lake. Structural field work was aimed at defining the deformation pattern around the caldera. The caldera consists of along-rim and across-rim structures, resulting from local and regional (maximum extension ~NE–SW) stress fields, respectively. These structures cross-cut each other at high angles, suggesting that the two stress fields remain distinct, each prevailing during rifting or caldera collapse. The local along-rim extensional fractures are gravity-driven structures that formed due to the retreat of the caldera wall after collapse, and are confined to the region of caldera subsidence. The across-rim structures are mainly located to the N and S of the caldera, where they form rift zones each accommodating a similar amount of extension (~6.3 m), but displaying different trends and extension directions. Analogue models of interacting fractures are consistent with the Southern Rift being representative of the regional fault kinematics, while the Northern Rift is a local perturbation, resulting from the interaction between two right-stepping rift segments along the Erta Ale Range.


*Keywords:* Fractures; Caldera; Rift zone; Afar; Erta Ale; Analogue models

## 1. Introduction

Deformation in volcanic areas is usually the result of the interaction between structures related to a regional stress field (far-field) and a local stress field (near-field). Regional structures are often associated with the generation and rise of magma, while local structures may result from the rise and emplacement of magma. The interplay between these two scales of structures are often best observed at calderas.

Calderas consist of depressions, whose diameters are several times larger than the diameter of vents (Williams, 1941), related to underpressure (Lipman, 1997) or overpressure (Gudmundsson, 1988) conditions within the underlying magma chamber. These extreme pressure conditions result in the development of a subcircular collapsed area, with maximum subsidence ranging from tens of metres (usually in mafic calderas) to a few kilometres (usually in felsic calderas). As the formation of calderas may be related to overpressure/underpressure conditions within the underlying reservoir, their shape can be similar to the map-view shape of the reservoir causing the collapse (Bosworth et al., 2003, and references therein).

The geometry of, and structures associated with, calderas reflect both the influence of a regional stress field (responsible for the generation and accumulation of magma in the underlying reservoir) and a local stress field, induced by the reservoir itself (Gudmundsson, 1998, and references therein). Calderas are usually found along continental and oceanic rift zones (Cole et al., 2005, and references therein), even though significant numbers have also been found in strike-slip (e.g. Bellier and Sebrier, 1994) and compressional settings (De Silva, 1989; Yoshida, 2001).

Defining the deformation pattern due to the local and regional stresses at calderas is particularly important for understanding how regional tectonics impact on their formation. Calderas are, for example, elongated at different trends with

* Tel.: +39 06 5488 8043; fax: +39 06 5488 8201.
*E-mail address:* acocella@uniroma3.it

0191-8141/$ - see front matter © 2006 Elsevier Ltd. All rights reserved.
doi:10.1016/j.jsg.2006.06.014

respect to the regional structures, from which it can be inferred that the tectonic controls on magma rise and emplacement are variable (Acocella et al., 2002; Holohan et al., 2005). Moreover, knowledge of the interplay between regional and local structures is an essential step for predicting the location of opening of a vent or a fissure during episodes of volcanic unrest. Despite these important issues and the large amount of studies on calderas (e.g. Cole et al., 2005, and references therein), the relationships between regional and local structures have been poorly studied to date (e.g. Minor, 1995; Bosworth et al., 2003). Investigating these relationships in well-exposed calderas may permit generic conclusions to be draw regarding the origin and development of calderas, which may be of benefit for future studies where caldera structures are complex or poorly exposed. Erta Ale, in northern Afar (Ethiopia), is an active basaltic caldera characterized by many well exposed faults and fractures and a complete lack of surficial vegetation or regolith cover (Fig. 1). Moreover, as Erta Ale caldera lies along the active North Afar Rift (Barberi and Varet, 1972; Tapponier et al., 1990), the regional tectonics can be investigated.

In order to study the surface deformation related to the collapse of the Erta Ale caldera and its relationship to the surrounding regional tectonics, we use structural field work, in the Erta Ale caldera area, and analogue experiments. Field work permits estimation of the geometries and kinematics of deformation at the surface. Erta Ale area is notoriously hard to reach. Access since the early 1970s has been restricted, due to the heavy political instability of the region; however, the slight improvement of the political situation permits now sporadic visits. The field analysis was undertaken during a 10-day helicopter expedition in December 2003. While field work provides information on the caldera structure and its tectonic environment, analogue experiments are exclusively devoted towards providing a better understanding of the regional tectonics in which the caldera has formed. With these tools, the present study aims to define: (1) the deformation pattern related to caldera collapse; (2) the regional structural setting of the caldera; and (3) how the superimposition between the regional and local stresses occurs. The data collected show that the two stress fields produce distinct deformation patterns.

## 2. Erta Ale caldera and its tectonic setting

Erta Ale caldera lies along the NNW–SSE trending Erta Ale Range, in the Danakil depression, northern Afar (Fig. 2; Barberi and Varet, 1970). Afar is a triple junction between the Red Sea, Aden and Ethiopian rifts (McKenzie et al., 1970; Tazieff et al., 1972; Le Pichon and Francheteau, 1978). The deformation pattern within Afar is, however, mainly the result of the interaction between the Red Sea and Gulf of Aden rifts, which forms a broadly deformed area characterized by bookshelf faulting and block rotations (Mohr, 1972; Tapponier et al., 1990; Manighetti et al., 2001).

Erta Ale Range is in the northern part of the NW–SE trending Red Sea Propagator, which is the on-land southern termination of the Red Sea Rift (Tazieff et al., 1972; Manighetti et al., 1998). The Ethiopian plateau (mean elevation ~2500 m above sea level) and the Danakil Alps (mean elevation ~1000 m above sea level) lie to the east and west, respectively, of the thinned crust in the propagator. This propagator is currently extending at ~2 mm/year due to spreading between the Nubia Plate and the Danakil Microplate, (Fig. 2; Jestin et al., 1994; Eagles et al., 2002). The axis of Erta Ale Range is characterized by active normal faulting and diffuse volcanism, which is


Fig. 1. Aerial view of the northern part of Erta Ale caldera, showing the caldera rim and the pit craters within the caldera which host the lava lakes. The arrow shows an example of an along-rim fracture. For a scale, the southernmost pit crater is ~90 m wide.

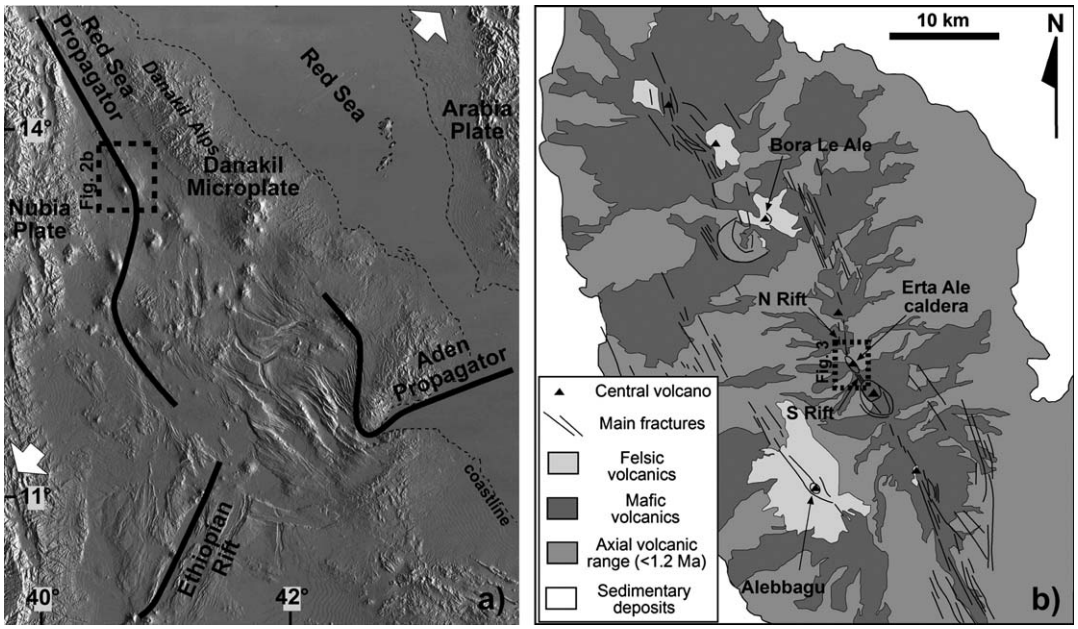


Fig. 2. (a) Tectonic setting of the Afar region; arrows show relative motion of the Nubia and Arabia plates (at N40°E, 16 ± 1 mm/year; from Manighetti et al., 2001, and references therein). (b) Geology and structure of the central part of Erta Ale Range (modified after Barberi and Varet, 1972).

mainly basaltic in composition, although fractional crystallization has produced some more evolved rocks (Fig. 2; Barberi and Varet, 1970, 1972; Barrat et al., 1998; Amelung et al., 2000). Erta Ale Range has a mean elevation of several hundred metres above sea level, rising above a plain of evaporite and lacustrine deposits, at a mean altitude of 200 m below sea level.

Erta Ale caldera is located along Erta Ale Range on the summit of a basaltic shield volcano, rising ~1000 m above the surrounding plain. The caldera consists of an elliptical depression, which trends NNW–SSE, has dimensions of approximately 1600 × 700 m, and may comprise several overlapping subcircular collapse events (Fig. 3; Oppenheimer and Francis, 1998). Erta Ale is most famous for its basaltic lava lakes, which are located within two pit craters in the northern part of the caldera, and have been intermittently active during the last century (Barberi et al., 1973; Oppenheimer and Francis, 1998). The mechanism by which lava feeds the lakes is still the subject of study (Harris et al., 2005). The lakes are associated with a low extrusion rate of lava, which suggests that the volcano mainly grows through intrusions (Oppenheimer and Francis, 1998) or, alternatively, that convection of recycled magma occurs (Oppenheimer et al., 2004), without significant plutonism (Harris et al., 1999).

## 3. Structural field data

Structural data have been mainly collected along the entire rim and outer border (up to a distance of ~1 km from the rim) of the caldera, as local collapses and recent lava flows within the caldera mask the original floor and the innermost structures. Nevertheless, the study along the rim and outer border permits the recognition of most of the structures possibly related to caldera collapse and to regional tectonics. These structures have been mapped and measured at a metre scale. Immediately outside the well-defined subvertical caldera wall (Fig. 1), which marks the caldera rim, two sets of structures have been recognized. The first set of structures comprise extensional fractures, which are usually parallel to, and a maximum distance of few tens of metres from, the rim. These

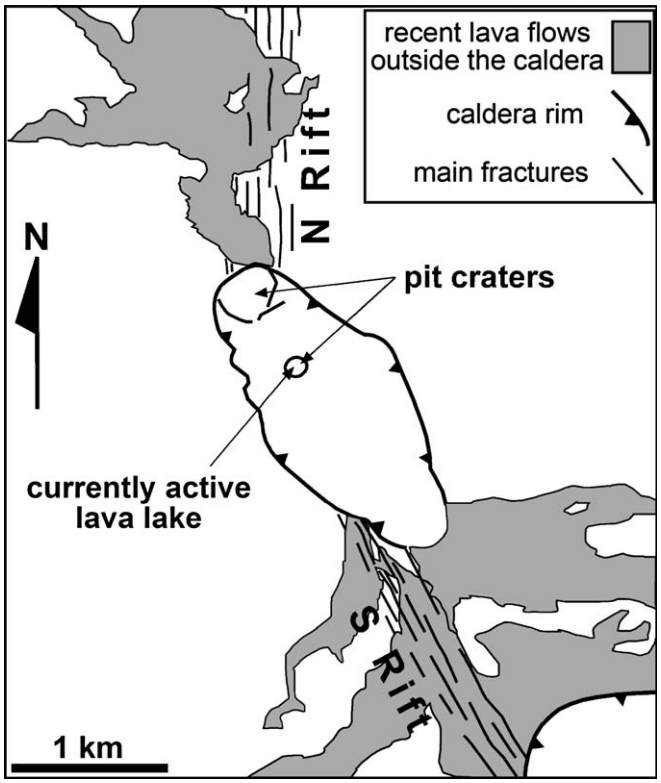


Fig. 3. Main features of the NNW–SSE elongated Erta Ale caldera.

fractures are found throughout the border of the caldera and are here referred to as along-rim structures (Fig. 1). The second set of structures consists of extensional fractures and normal faults, which usually strike at a high angle to the trend of the caldera rim and extend a considerable distance (up to a few kilometres) outside the caldera. These structures are only found in narrow zones at the northern and southern tips of the caldera and are here referred to as across-rim structures. These structures are subradial to the caldera and, within the caldera, are covered by recent lava flows.

### 3.1. The caldera wall

The caldera wall is completely exposed and consists of a continuous subvertical scarp with a variable height of between ~80 and a very few metres (Fig. 1). The wall almost entirely comprises a homogeneous pile of subhorizontal basaltic lava flows. The scarp is characterized by an irregular surface, locally shaped by leaning boulders of lava, and does not form a continuously polished plane (Fig. 4a). As the caldera fault was not visible, no kinematic indicators or slickensides could be measured. The height of the scarp generally increases as it gets closer to the central part of the caldera, and is lowest at its northern and southern limits. In addition to this general pattern, the variable height of the scarp may locally depend on the presence and thickness of more recent lava flows within the caldera which abut, and partially bury, the caldera wall.

### 3.2. Along-rim structures

The along-rim extensional fractures of the caldera, already described by Barberi and Varet (1970), are always parallel to the rim (Fig. 4b). These, as measured on the field, have an overall ~NW–SE strike, peaking at N48°W, although other minor orientations are observed (Fig. 5a). This mean orientation is approximately parallel to the ~NW–SE elongation direction of the elliptical caldera rim. The distance of fractures from the rim and the amount of opening of these along-rim fractures varies considerably. Usually, they are found within 20 meters of the rim, although some extend up to 60 m from the rim. There is a positive relation between the maximum distance of the fractures from the caldera rim and the height of the caldera scarp (Fig. 5b). This suggests that higher caldera scarps are associated with wider zones of fracturing outside the rim. The opening width, or dilation, of these extensional fractures varies from a few tens of centimeters to a few metres. There is a general tendency for the fractures to have greater dilation when they are nearer to the caldera rim.

### 3.3. Across-rim structures

The across-rim structures, which are evidently a significant distance (few km) outside the caldera rim, cluster to the north and south of the caldera.

Outside the northern rim, the structures are concentrated within a ~N–S trending fracture zone, which is ~1 km wide and locally buried by recent lava flows (Fig. 6). This fracture zone consists of segments of subparallel extension fractures and, subordinately, of normal faults (Fig. 7). Hornitos are sometimes located along fractures traces. The extensional fractures have variable lengths and opening widths of typically up to several hundreds of metres and a few metres, respectively. The normal faults are usually 1 km long, with a maximum vertical displacement of a few metres. The mean strike of all the extensional fractures and normal faults is N3°E, while the mean opening direction for the fractures is N76°W (Fig. 8). The opening direction was obtained by measuring the direction given by matching asperities on the opposing walls of fracture planes (see Acocella and Korme, 2002). The non-orthogonality (11° of difference) between the mean strike of the fractures and the trend of their mean extension direction implies an overall moderate component of dextral shear along the fracture zone on the northern rim of the caldera. The total amount of extension across this fracture zone was measured by summing all the horizontal and vertical components of displacement along two ~E–W profiles (traces in Fig. 6). The profiles were oriented perpendicular to the overall

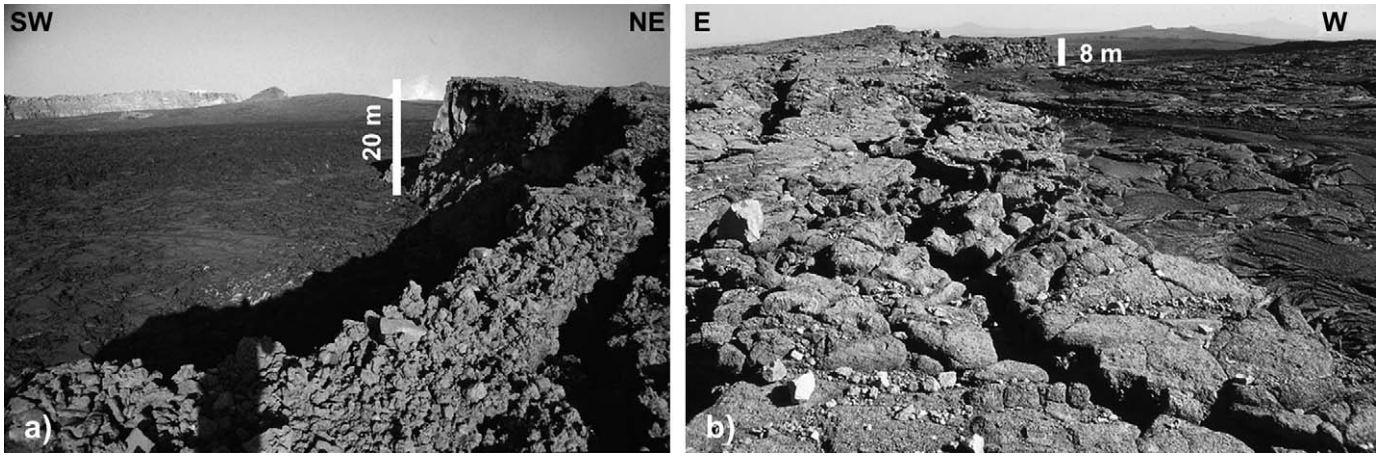


Fig. 4. (a) View of the SE part of the caldera wall. (b) Extensional fractures parallel to the caldera wall on the outer north rim of the caldera.

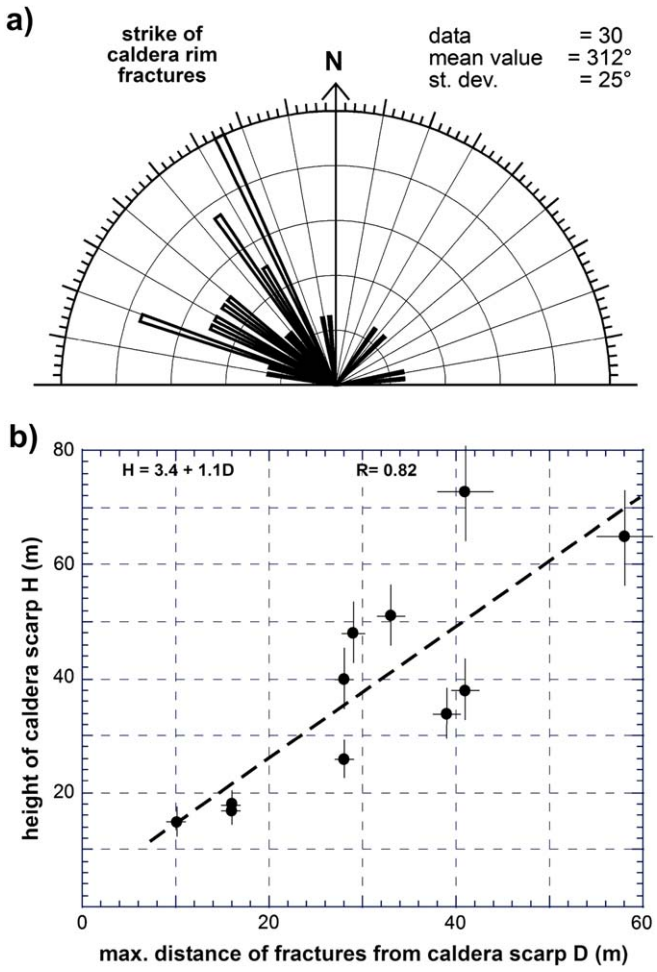


Fig. 5. (a) Orientation of the along-rim extensional fractures. (b) Linear relation between the maximum distance from the caldera rim at which the fractures have been found (D) and the height of the caldera wall (H) for 11 sites.

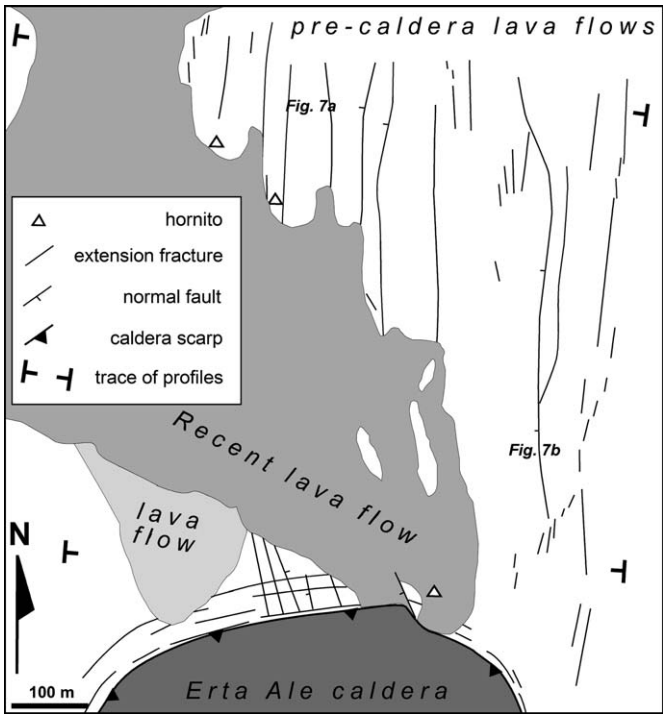


Fig. 6. Structural sketch of the northern outer rim of Erta Ale caldera, highlighting a ~N–S fracture zone formed by across-rim structures. Along-rim fractures are present immediately adjacent to the Erta Ale caldera in the south of the map area.

trend of the fracture zone and cross the highest strained parts of the zone. The profiles include data from fractures lying within a ~100 wide zone parallel to the profiles. This procedure gives a total extension of 753 cm for the northern profile (line A, Fig. 6) and 837 cm for the southern profile (line B, Fig. 9). The mean extension for both profiles is $8 \pm 0.6$ m.

To the south of the caldera, structures cluster along a ~NNW–SSE trending fracture zone, several hundred metres wide, which is partly buried by more recent lava flows (Fig. 9). This fracture zone consists of segments of subparallel extensional fractures. These fractures are close in location and orientation to basaltic fissure eruptions formed by several hornitos aligned ~NNW–SSE (Figs. 9 and 10). The extensional fractures have a variable length and opening width, which are usually up to 1 km and a few metres, respectively. Their mean strike is N20°W, whereas their mean opening direction is N68°E (Fig. 11). In this case, as the extension direction of the fracture zone is almost perpendicular (difference of 2°) to its mean strike, the fracture zone formed due to orthogonal extension. The total amount of extension across the southern fracture zone was obtained by summing all of the horizontal displacements along two ~E–W profiles (traces in Fig. 9). This gives a total extension of 580 cm for the northern profile (line C, Fig. 9) and 677 cm for the southern profile (line D, Fig. 9), with a mean extension of $6.3 \pm 0.5$ m.

## 4. Interpretation of the field data

### 4.1. Along-rim structures and caldera wall

Even in the most favourable exposure conditions of Erta Ale, it is not possible to determine whether the observed caldera wall corresponds to the original caldera fault, or whether it is an 'erosional' feature accommodating displacement of a buried fault inside the caldera. In either case, the lack of a polished fault plane with slickenlines indicates that a dilational component of displacement accompanied the development of the present caldera wall. Therefore, if the caldera wall corresponds to the principal caldera-forming fault plane, then this fault must accommodate both vertical and horizontal (i.e. tensile) components of displacement. The possibility of tensile displacement during caldera collapse is now tested.

Calderas are usually inferred to be bound by inward dipping normal faults (Gudmundsson, 1988) or by outward dipping high-angle reverse faults (Marti et al., 1994; Acocella et al., 2000a; Roche et al., 2000; Walter and Troll, 2001). Calderas bordered by inward dipping normal faults are unlikely to be associated with a component of dilation along a subvertical wall, as the lithostatic pressure will hinder the formation of extensional fractures along inward dipping planes. Moreover, the subvertical caldera wall at Erta Ale is not consistent with an

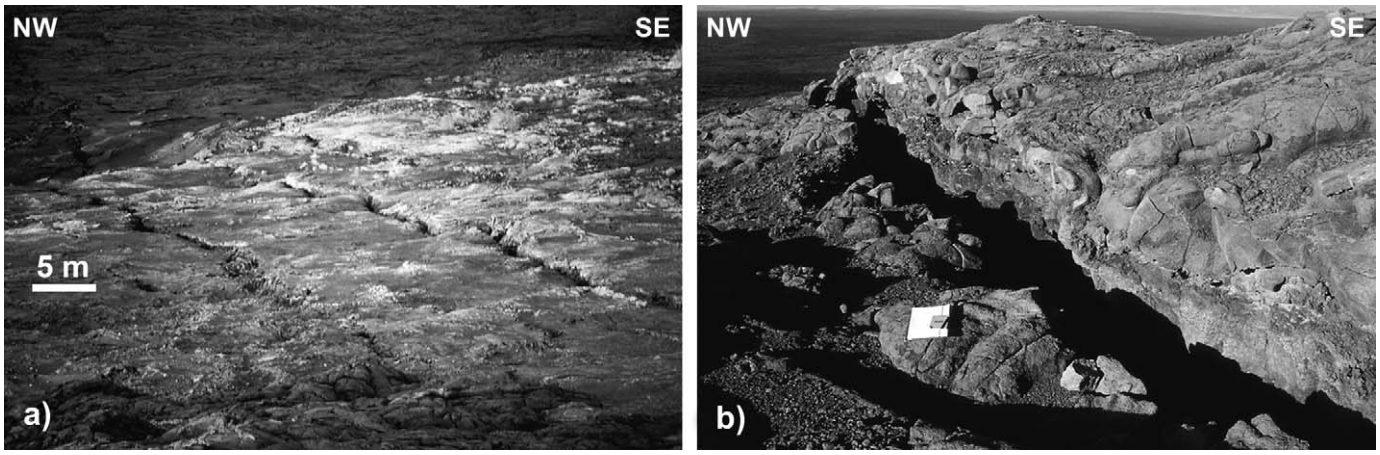


Fig. 7. (a) N–S extension fractures on the N rim of the caldera. (b) Small (throw ~1 m) ~N–S open normal fault on the N rim of the caldera. Location of structures shown in Fig. 6.

inward dipping fault. In the case of outward dipping high angle reverse faults bordering the caldera, the downward movement of the central block may create, at least at the surface (Gudmundsson, 1992), tensile conditions, consistent with that observed on the caldera wall. Nevertheless, as there is no evidence of an outward dipping caldera wall at Erta Ale, the formation of the observed caldera wall as a direct result of caldera collapse is unlikely. The third possible origin of dilation is that the caldera wall coincides with a subvertical fault plane, which also seems unlikely, as no polished fault plane with slickenlines was observed. Therefore, it is suggested that the caldera wall does not correspond with the caldera fault; rather that it corresponds to an 'erosional' feature masking an underlying fault plane or unknown orientation and inside the present caldera wall.

The extensional fractures found along the caldera rim can be interpreted as resulting from the collapse of the caldera scarp. In fact, these fractures are always parallel to the rim, bordering it for the entire perimeter. Moreover, they are found within a distance proportional to the scarp height; suggesting that higher scarps may mobilize larger masses outside the rim and that the along-rim anelastic deformation does not usually propagate beyond the region of caldera subsidence. Therefore, extensional fractures may be (a) collapse structures directly induced by the subsidence of the caldera, or (b) gravity structures resulting from the lack of confinement induced by the progressive gravitational collapse of the caldera wall. The fact that the extensional fractures are not characterized by a significant component of shear suggests that the second scenario is more likely. Although these fractures are likely

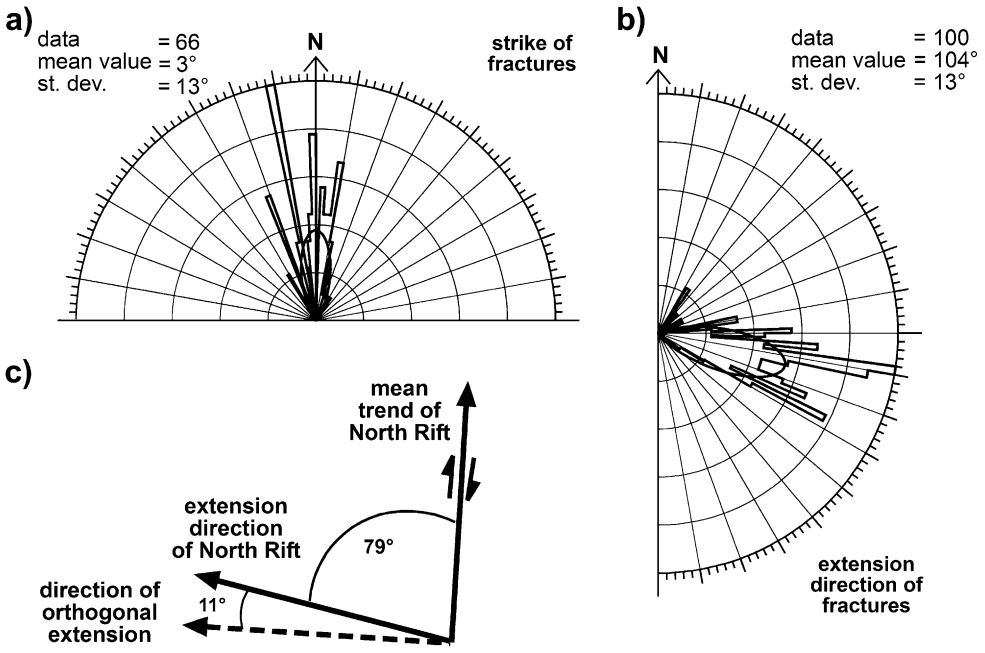


Fig. 8. Orientation (a) and opening direction (b) of across-rim fractures on the N rim of the Erta Ale caldera. The 79° angle between the fracture strike and extension direction suggests a dextral component of shear (c).

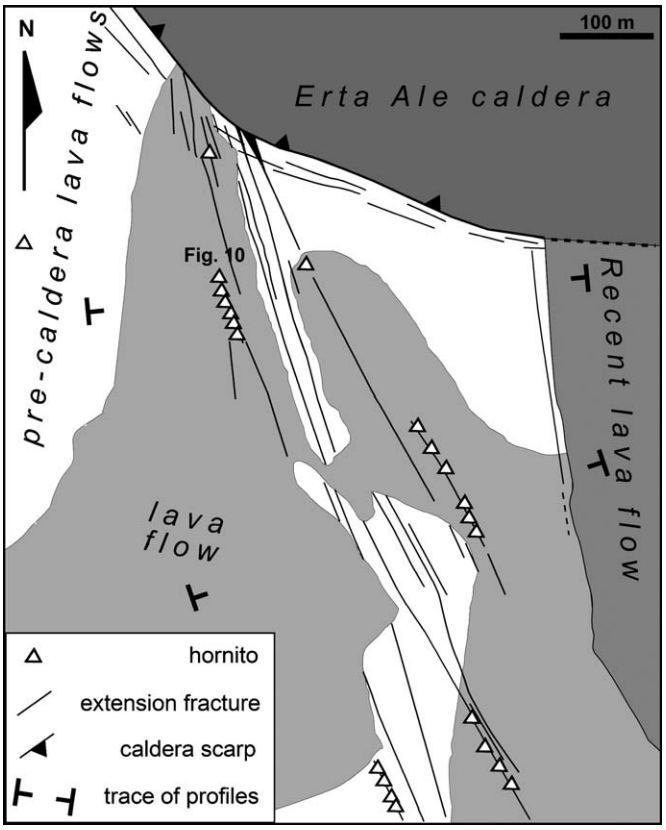


Fig. 9. Structural sketch of the southern outer rim of the Erta Ale caldera, highlighting a ~NNW–SSE fracture zone formed by across-rim structures. Along-rim fractures are present immediately adjacent to the Erta Ale caldera in the north of the map area.

to be gravitational in origin, it is noteworthy that the extensional fractures along the caldera rim form as an indirect result of the local stress field responsible for caldera collapse. Therefore, despite a significant gravitational component, the development of the along-rim structures can be indirectly related to local tectonics.

A possible model for the evolution of the caldera wall, as well as of the associated extensional fractures along the outer rim, is proposed in Fig. 12. In a first stage, the activity of the caldera fault determines the gravitational instability of the overlying wall. Extensional fractures form in an outer portion because of the lack of confinement of the caldera wall (Fig. 12a). Following the collapse of the inner block, the zone of extensional fracturing along the rim widens outwards away from the centre of the caldera (Fig. 12b). This mechanism suggests progressive widening of the caldera through the enlargement and collapse of portions of its wall.


Fig. 10. NNW–SSE extension fracture filled by a lava flow erupted from a hornito located along the NNW continuation of the fracture. See Fig. 9 for location.

### 4.2. Across-rim structures

Across-rim structures concentrated north and south of the caldera in areas of intense volcanic activity. In analogy to other basaltic calderas, e.g. Hawaii (Walker, 1990, and references therein), these fractures form rift zones (Figs. 2, 6 and 9). Because the rift zones are well outside the caldera, they can be related to the regional stress field. These rift zones cross-cut the along-rim structures at a high angle, suggesting a lack of mechanical interaction between the two types of structures. This implies that, where both structures are present, their stress fields remain distinct, without merging. Therefore, it is inferred that the stress field in these areas varies temporally, with one dominant mechanism (rifting or caldera collapse) acting at a given time.

Both rifts have accommodated a similar amount of total extension, with values ranging between 6.3 and 8 m. The S Rift is undergoing pure extension, while the N Rift accommodates a minor component of dextral shear; which, given the total amount of extension, corresponds to ~1.5 m or to ~20% of the total strain. Differences in the obliquity of extension across each rift are generally consistent with their dissimilar orientations relative to the regional extension direction. The S Rift is subparallel to the trend of Erta Ale Range structures (Barberi and Varet, 1972), while the N–S trending N Rift is slightly oblique to regional structures. Despite an overall regional control on the N rift, both its trend and extension direction represent a minor departure from the regional patterns within the Erta Ale Range.

A detailed study of the structures along the Erta Ale Range shows that this consists of discrete ~NNW–SSE trending tectonic rift segments associated with volcanic activity (Fig. 2). To the south of Erta Ale, the S Rift coincides with the northernmost part of the ~NNW–SSE trending Erta Ale rift segment (Fig. 2). To the north of Erta Ale, the axis of tectonic and volcanic activity shifts to the NE, along a dextrally offset segment of the rift axis (Fig. 2). Further north, tectonic and volcanic activity shifts back to the SW along the northern continuation of the Erta Ale segment, which is referred to as the Bora Le Ale segment. Therefore, the N–S structures along the N Rift may be interpreted as local structures within the transfer zone between the two dextrally offset rift segments. In order to test the model that the N Rift and its extension direction are induced by the interaction of two offset extensional segments and to understand better the tectonic controls on the caldera, results from new analogue models are analysed. These

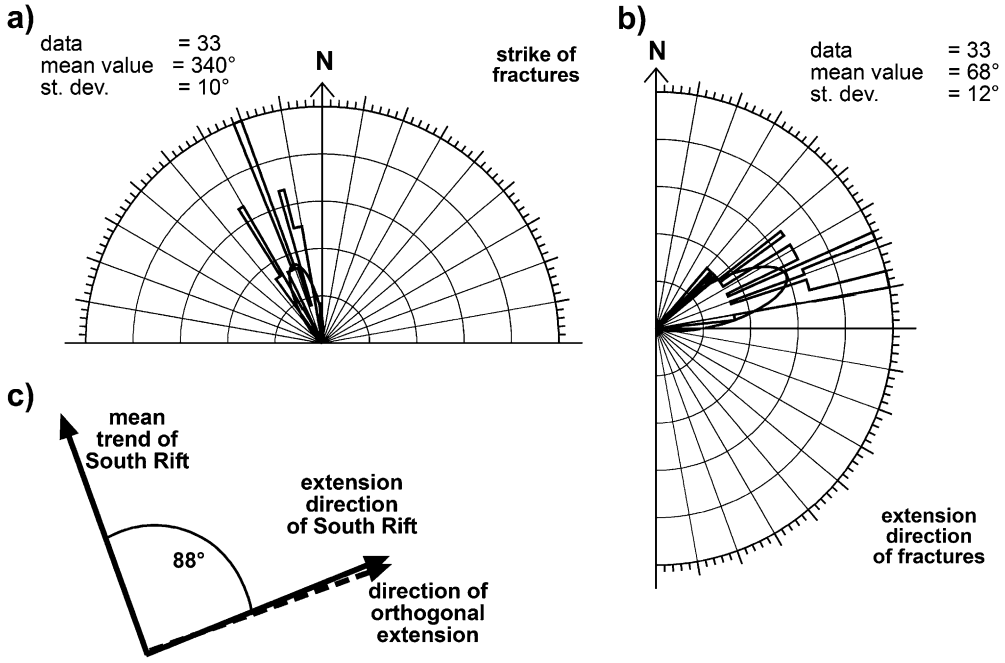


Fig. 11. Orientation (a) and opening direction (b) of the across-rim fractures on the S rim of the Erta Ale caldera. The 88° angle between the fracture strike and extension direction suggests extension orthogonal to the fractures (c).

experiments are exclusively used for a better definition of the tectonic setting of the caldera.

## 5. Analogue modelling of interacting offset segments

### *5.1. Scaling, materials, experimental set-up and assumptions*

In order to simulate the growth of rift zones related to the rise of magma, the experiments were performed in a centrifuge, similar to previous studies (e.g. Mulugeta, 1985). The experiments simulated the interaction of two offset rift segments formed in conjunction with the rise of hot asthenosphere within a thermally anomalous mantle below a thinned lithosphere. The rheology of the lithosphere has been approximated with an overall brittle behaviour (Ranalli, 1995).

The length ratio $z^*$ between model and nature is $10^{-7}$ (1 cm in the model corresponds to ~100 km in nature; Table 1). The densities of the rocks of the crust and upper mantle (2600–2900 kg m$^{-3}$) and of the available experimental materials (900–1800 kg m$^{-3}$) impose a density ratio of $\rho^* \sim 0.5$. Since the models were run at $\sim 10^2$ $g$, the gravity ratio is $g^* = 10^2$. These ratios imply that the stress ratio between the model and nature is $\sigma^* = \rho^* g^* z^* \sim 5 \times 10^{-6}$ (Table 1). For these dimensions of stress and a mean cohesion for the rocks $c \sim 10^7$ Pa (Ranalli, 1995), the cohesion of the lithosphere, must be scaled at $\sim 5 \times 10^{-6}$; with a low cohesion material ($c \sim 50$ Pa) required to simulate the oceanic lithosphere. For this purpose, we used a mixture of Vaseline (60%), paraffin (20%) and gypsum powder (20%), with cohesion of a few hundred Pa. The cohesion of the material was evaluated through shear tests, using Casagrande's box.

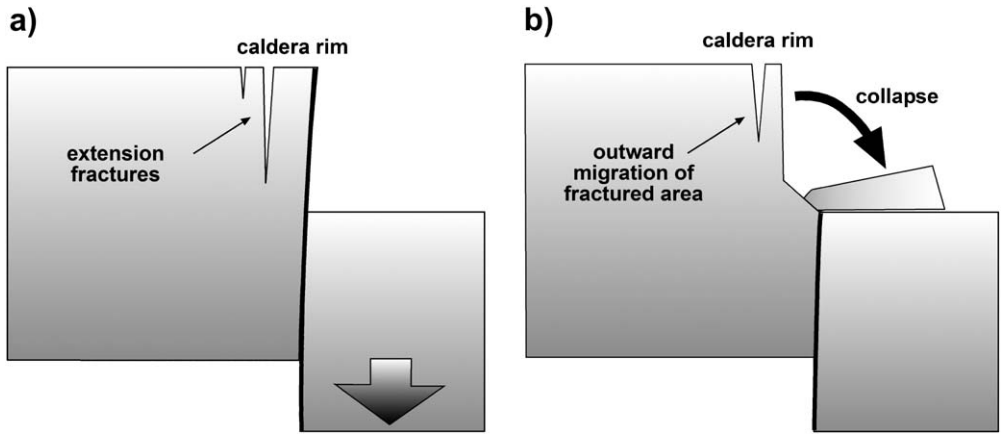


Fig. 12. Mechanism of development of the caldera wall. See text for further details.

Table 1
Scaling ratios between analogue models and nature

| Parameter | Model/Nature ratio |
|---|---|
| Length | $L^* \sim 10^{-7}$ |
| Density | $\rho^* \sim 0.5$ |
| Gravity | $g^* \sim 10^2$ |
| Stress | $\sigma^* \sim 5 \times 10^{-6}$ |
| Viscosity | $\mu^* \sim 10^{-14}$ |
| Strain rates | $\varepsilon^* \sim 10^{-12}$ |
| Time | $t^* = 1/\varepsilon^* \sim 10^{12}$ |

Newtonian silicone (LSI), with density = 1310 kg m$^{-3}$ (measured in a densimeter based on Archimedes' law) and viscosity $\mu \sim 3 \times 10^4$ Pa s (measured in a Couette viscosimeter; Weijermars, 1986), simulated the thermally anomalous asthenosphere. The surrounding mantle was simulated using a denser and more viscous silicone (DSI; density = 1410 kg m$^{-3}$; viscosity $\mu \sim 7 \times 10^5$ Pa s). The mean viscosity of a thermally anomalous asthenosphere in nature is $\mu \sim 10^{19}$ Pa s and that of the surrounding mantle is $\mu = 10^{20}$–$10^{21}$ (Ranalli, 1995). Therefore, the density (~100 kg m$^{-3}$) and viscosity (~50 Pa s) contrast between the LSI and DSI are consistent with those found in nature. The LSI and DSI were ~1 cm and ~2 cm thick respectively, to simulate a mean thickness (in the order of $10^2$ km) of the lithosphere and asthenosphere, consistent with the imposed length ratio $z^*$ (Fig. 13). The mean strain rates related to the rise of asthenosphere in nature are $\varepsilon_n \sim 10^{-15}$ s$^{-1}$ (Turcotte and Schubert, 2002), whereas in the experiments they are $\varepsilon_m \sim 10^{-3}$ s$^{-1}$, giving a strain rate ratio between the model and nature of $\varepsilon^* = 10^{-12}$ (Table 1). As the time ratio between the model and nature is $t^* = 1/\varepsilon^* \sim 10^{12}$ (Table 1), 1 s in the experiment corresponds to $3.3 \times 10^4$ years in nature, implying that the mean duration of the experiments (~5 min) simulates ~$10^7$ years in nature.

These materials were introduced to a centrifuge with the configuration shown in Fig. 13. The LSI is embedded within the DSI, forming two offset parallelepipeds. Two en-echelon cuts, with $c \sim 0$ Pa, were made within the brittle material before the run along the centre of the LSI parallelepipeds (Fig. 13). Different configurations for the en-echelon fractures were tested, varying their overlap width, overlap length, length and strike. The centrifuge induced, through a density contrast, the rise of the LSI through the DSI. The rise of the LSI beneath the two fractures enhanced their along-strike propagation and thus interaction.

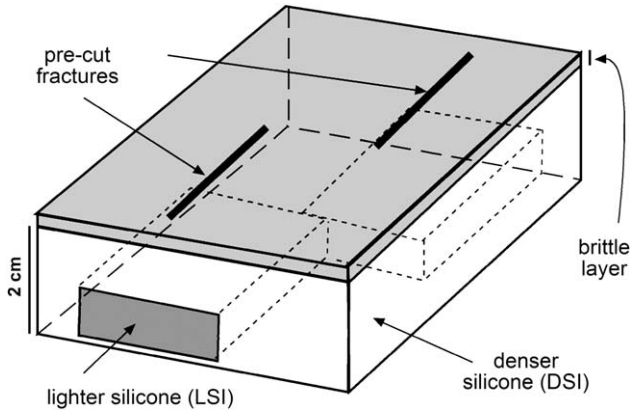


Fig. 13. Analogue models experimental set up.

This set-up is similar to previous studies (Corti et al., 2003, and references therein; Tentler, 2003), and avoids the limitations produced by basement discontinuities commonly found in the interaction zone when simulating offset extensional segments (Mauduit and Dauteuil, 1996; Acocella et al., 1999).

The following assumptions have been made in order to interpret the models. (a) The scale at which the growth of ridge segments has been simulated (hundreds of km) is one order of magnitude larger than that required by the natural case (tens of km); this imposes a $z^*$ (length ratio between model and nature) one order of magnitude lower than expected. Such a length ratio has been chosen to maintain the proper viscosity proportions between experiments and nature. In fact, only the $z^*$ value used permits simulation of the correct viscosity contrast between the rising magma and the surrounding medium. As the interaction mechanism along rift zones is scale independent from metres to hundreds of kilometres (Acocella et al., 2000b), such a simulation of a scale larger than required is considered a reasonable first approximation. (b) The growth of the cracks in the experiments is enhanced by the rise of the magma analogue, consistent with what has been observed at oceanic ridges. It is presently not well constrained whether the growth of the Red Sea Propagator is driven by the rise of magma (as in the experiments) or by tectonics only. However, as its overall evolutionary stage is closer to that of oceanic rifts, rather than continental rifts (Hayward and Ebinger, 1996), the rise of hot magma is expected to contribute significantly to the growth of the Rift. For this reason, the experimental simulation of the growth of the Red Sea Propagator through the rise of magma appears feasible. (c) The aim of the experiments is not to simulate a specific case, as the difficulty of determining its natural parameters would limit the applicability of the models. Rather, the goal is to understand the overall mechanism of interaction, so that it might be applied to a wide range of natural cases, including the Erta Ale Range.

### 5.2. Description and discussion of the experiments

Thirty-three experiments were carried out to study how rift-zone segments with variable geometries (e.g., overlap length, overlap width or overstep, length and orientation) grow and interact. A detailed description of all experiments is beyond the scope of this paper. The experiments all produced the same general evolution and mechanism of fracture interaction, which is here summarized with reference to the model generated in experiment OFC 12 (Fig. 14). This experiment had an initial configuration of fractures similar to that of the offset rift segments within Erta Ale Range. In fact, the initial configuration of the two parallel fractures in OFC 12 is $S$ (overstep) = 0.5 cm and OL (overlap length) = −1 cm (Fig. 14a). Therefore, the aspect ratio $A$ (where $A = \mathrm{OL}/S$) of the resulting interacting zone is ~2 (absolute value), similar to that between the Erta Ale segment and the rift segment to the NE (Fig. 2b).

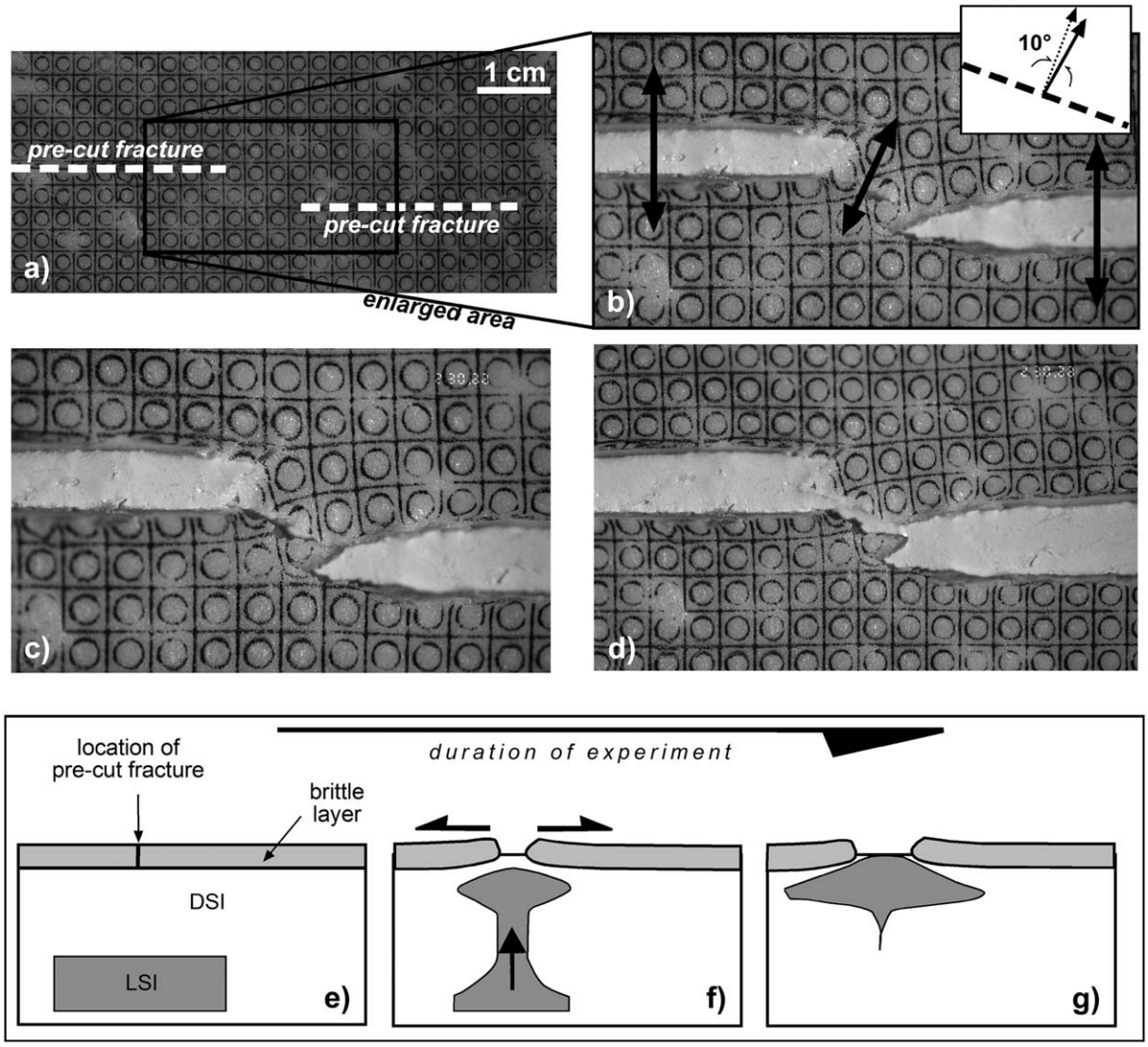


Fig. 14. Evolution of experiment OFC 12. (a) Map view of undeformed stage. The pre-cut fractures are highlighted by the dashed lines. (b–d) Map view enlargement of the central part of the experiment. (b) Experiment at $t = 4'$; the extension directions of the primary fractures and in the interaction zone are highlighted (arrows). Upper inset to the right shows the angular relationships between the connecting fracture (dashed line), its extension direction (solid arrow), and the direction of orthogonal extension (dotted arrow): the discrepancy between the two arrows suggests a minor ($\sim 10^\circ$) component of dextral shear. In these calculations the minor counter-clockwise rotation observed in the model (see text for further details) has been removed. (c) Experiment at $t = 4'$; a connecting fracture develops. (d) Experiment at $t = 5'$; a single continuous fracture is formed. Schematic cross-sections of the experiment are shown at the undeformed stage (e), during the rise of the LSI (f) and for the final emplacement (g) of LSI.

The undeformed model, at $t = 0'$ (minutes) is shown, in map view (Fig. 14a); a reference grid is placed on the surface of the model. At $t = 4'$, the two fractures widen and propagate along their strike, producing an enlargement of the area of interaction between the fractures (Fig. 14b). The interaction zone is characterized by moderate clockwise rotations about vertical axes, as shown by the distortion of the reference grid. These rotations are consistent with a local opening direction at $\sim 30^\circ$ to the overall opening direction, which is perpendicular to the trend of the primary fractures. At $t = 4'$, the interaction of the fractures is also marked by the incipient development of a connecting fracture at an oblique angle ($\sim 20^\circ$) to the trend of the primary fracture. At $t = 5'$, the two parent fractures, as well as the connecting fracture at oblique angle, further propagate due to the increased extension. Moreover, the connecting fracture further propagates along-strike (Fig. 14c). The rotations about vertical axes in the interaction zone do not increase, suggesting that most of the elastic strain is accommodated before the development of the connecting fracture. At $t = 6'$, the model reaches its mature configuration (Fig. 14d). This is characterized by the complete propagation of the connecting fracture, which now intersects both primary fractures. At this stage, the connecting fracture displays a significant amount of opening. Any increase in the duration of the experiment leads to further opening of the sinuous structure obtained so far, which behaves as a single, continuous system.

The evolution of the experiment in section view is shown in the line drawings in Fig. 14e, f and g. These drawings have been obtained by merging the section views of this and other experiments with a similar configuration. At the undeformed

stage, the LSI is placed within the DSI, beneath the pre-cut fractures in the brittle material (Fig. 14e). The centrifuge induces, as a consequence of the increased density contrast, the rise of the LSI at the base of the pre-cut fractures (Fig. 14f). Due to the rise of the LSI the fractures widen (in section) and propagate (along-strike). The mature stage is characterized by the almost complete rise of the LSI within the DSI at the base of the brittle material (Fig. 14g); the fractures are wider, with the LSI partly filling the space created by the fractures and reaching the surface.

A detailed discussion of the whole experimental set and its implications is beyond the purpose of this study; also, as all the experiments show an evolution consistent with the one of OFC 12, only the results and implications of this experiments will be discussed here. Along-strike propagation on the primary fractures is responsible for the interaction of the two en-echelon fractures, creating an overlap zone. The overlap zone is initially characterized by elastic deformation and later by an anelastic response. The former is shown by the local clockwise variation in the extension direction, which differs from the regional extension direction by up to ~30° (maximum stretching direction of the circles on the grid). Anelastic deformation is characterized by the development of the connecting fracture, almost perpendicular to the local extension direction within the interaction zone. The model undergoes a progressive general counter-clockwise rotation of the extension direction (see the increasing non-alignment between the grid lines at the sides of the parent fractures; Fig. 14), which is due to the imperfect confinement of the model within the centrifuge, and must be removed in order to estimate the opening direction of the connecting fracture. This rotation has been removed in Fig. 14b (and related inset), which shows the true kinematics of the connecting fracture. As the connecting fracture strikes at an angle of ~20° to the primary fractures, it strikes at ~30° to the overall extension direction. This implies a moderate (~10°) component of dextral shear associated with the opening of the connecting fracture. The presence of such moderate horizontal shear has been commonly observed within interaction zones (Acocella et al., 2000b, and references therein). Only when the connecting fracture reaches the two primary fractures, forming a single sinuous structure, can the interaction process be considered complete. At this stage, the single structure reaches a stable geometric and kinematic state.

In the experiments, the widening of the fractures (former lithosphere) is not compensated for by the creation of new lithosphere, which is inconsistent with what can be observed in nature. As creation of new lithosphere cannot be experimentally reproduced, the presence of silicone between the fractures should not be interpreted to indicate the occurrence of mantle exhumation along the ridges in nature.

### 5.3. Comparison between experiments and nature

The field data collected along the N and S Rift of Erta Ale show a discrepancy in the orientation and opening direction between the two rifts. This is inferred to result from the overall configuration of the rift segments along the Erta Ale Range. In particular, The Erta Ale segment and its neighbour segment to the NE show a dextral offset. This configuration may induce local variations in the orientation and opening direction between the two segments, which may be reflected in geometry and kinematics of the rift at the northern end of the caldera. Analogue models of interacting fractures simulate the interaction of offset ridges characterized by extension and by the rise of magma, similar to the conditions observed along the Erta Ale Propagator. The experimental results show that the interaction between offset fractures may develop connecting fractures with a different orientation and extension direction to the primary fractures. For a configuration similar to that of the rift segments along Erta Ale Range, the experimental connecting fracture has an obliquity of ~20° to the trend of the primary fractures, an extension direction at ~30° to the mean 'regional' extension direction, and a ~10°component of dextral shear. These modelling results are similar to the observations from Erta Ale, where the difference in the trend between the N and S rifts, comparable to the difference in trend between the connecting fracture and its parent, is 23°. Moreover, the difference in the extension direction between the N and S rifts, comparable to the difference in the extension direction between the connecting fracture and a primary fracture, is 36°. Finally, the component of dextral shear along the N Rift, comparable to that of the connecting fracture, is 11°.

The consistency between experimental and field data suggests that the N Rift results from the interaction between the Erta Ale segment and the segment immediately to the NE (Fig. 15). This interaction induces local variations in the trend of the N Rift, as well as in its opening direction. Conversely, the geometry and kinematics of the S Rift are considered representative of the Erta Ale segment, with an overall N20°W orientation and N68°E opening direction. Although not completely consistent with the estimated extension direction between Africa and Arabia (Fig. 2a), the measured extension direction of the S Rift is consistent with previous estimates along the Red Sea Propagator (Eagles et al., 2002). Therefore, the extension direction of the S Rift of Erta Ale may be representative of the present spreading direction between the Nubia Plate and Danakil Microplate.

The agreement between the experimental and natural data suggests that the N and S rifts at Erta Ale are the result of regional tectonics. It cannot, however, be discounted that a significant part of the observed deformation may also be due to the lateral emplacement of radial dikes from the caldera towards the lower slopes of the Erta Ale caldera, similar to that observed at other volcanoes (Acocella and Neri, 2003, and references therein). In fact, the emplacement of dikes, under certain conditions (Gudmundsson and Loetveit, 2005, and references therein) may produce extensional fractures and normal faults at the surface (Rubin and Pollard, 1988), similar those observed along the N and S rifts. At Erta Ale, the lateral emplacement of the dykes is also supported by the common association between the fractures and aligned vents or hornitos, especially in the S Rift. Although a significant portion of the observed deformation in the rifts may have been induced by

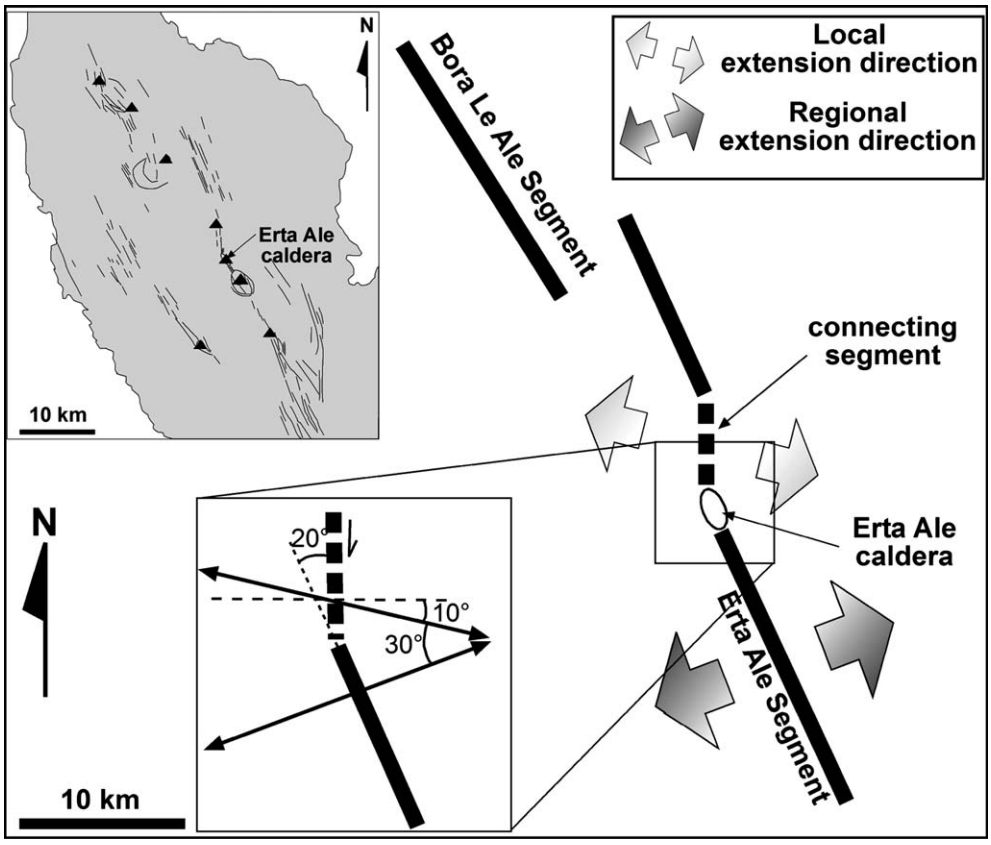


Fig. 15. Major tectonic and volcanic segments along the central Erta Ale Range (same area as Fig. 2b, which appears, reduced, in the inset) and their geometric and kinematic relationships. The connecting segment (N Rift) is characterized by a local extension direction, different to that of the Erta Ale segment (S Rift). Inset shows the consistent angular relationships found in the field and in the models: ~30° is the difference between the two extension directions, ~20° is the difference between the trend of the two segments and ~10° is the difference between the extension direction of the connecting segment and the direction orthogonal to it, i.e. the amount of dextral shear.

dike intrusion, emplacement of these dikes was still controlled by the regional stress field, as summarized in Fig. 15.

The amount of spreading between the two Nubia and Danakil plates has been estimated at ~2 mm/year (Jestin at al., 1994). Assuming that the axis of Erta Ale Range accommodates all of the spreading and using extension of 7 m (mean value of the N and the S rifts) across the axis of the range, the fractures observed in the N and S rifts may have formed in the last 350 years. This is a minimum estimate, as it is unlikely that all of the spreading between the Nubia and Danakil plates has been accommodated along the axis of the Erta Ale Range.

## 6. Conclusions

Field and analogue data define local and regional deformation patterns at Erta Ale caldera. The caldera is characterized by along-rim and across-rim structures, which result from the local and regional stress fields, respectively. These two sets of structures cross-cut each other at high angles, suggesting that the two stress fields remain distinct and prevail during rifting or caldera collapse. Along-rim fractures are gravity-driven and form due to the retreat of the caldera wall after caldera collapse. Their location suggests that the along-rim anelastic deformation does not usually propagate beyond the region of caldera subsidence. Across-rim normal faults and dilational fractures are concentrated in rifts at the northern and southern end of the caldera. The two rifts display different orientations and extension directions. Analogue models of interacting fractures suggest that the S rift is representative of the regional tectonic kinematics, while the N rift exhibits a local deviation from regional tectonics, resulting from the interaction between two offset rift segments along the Erta Ale Range.

## Acknowledgements

F. Barberi and R. Funiciello provided constant encouragement throughout the work. A. Nicol gave a critical reading of the manuscript and significantly improved the English. The field work was done in pleasant collaboration with R. Carniel. The analogue experiments were performed at the Hans Ramberg Tectonic Laboratories in Uppsala (Sweden). Previous experimental work from T. Tentler permitted to promptly evaluate the best set-up for the experiments. C. Talbot and G. Mulugeta provided useful suggestions during the experimental work. K. Benn and G. Stuart provided helpful reviews. Funded with MIUR 2003–2004 funds (F.B. responsible).

## References


Acocella, V., Korme, T., 2002. Holocene extension direction along the Main Ethiopian Rift, East Africa. Terra Nova 14, 191–197.

Acocella, V., Neri, M., 2003. What makes flank eruptions? The 2001 Etna eruption and its possible triggering mechanisms. Bulletin of Volcanology 65, 517–529.

Acocella, V., Faccenna, C., Funiciello, R., Rossetti, F., 1999. Sand-box modelling of basement controlled transfer zones in extensional domains. Terra Nova 11, 149–156.

Acocella, V., Cifelli, F., Funiciello, R., 2000a. Analogue models of collapse calderas and resurgent domes. Journal of Volcanology and Geothermal Research 104, 81–96.

Acocella, V., Gudmundsson, A., Funiciello, R., 2000b. Interaction and linkage of extension fractures and normal faults: examples from the rift zone of Iceland. Journal of Structural Geology 22, 1233–1246.

Acocella, V., Korme, T., Salvini, F., Funiciello, R., 2002. Elliptic calderas in the Ethiopian Rift: control of pre-existing structures. Journal of Volcanology and Geothermal Research 119, 189–203.

Amelung, F., Oppenheimer, C., Segall, P., Zebker, H., 2000. Ground deformation near Gada Ale volcano, Afar, observed by radar interferometry. Geophysical Research Letters 27, 3093–3096.

Barberi, F., Varet, J., 1970. The Erta Ale Volcanic Range (Danakil depression, northern Afar, Ethiopia). Bulletin Volcanologique 34, 848–917.

Barberi, F., Varet, J., 1972. Geological map of the Erta Ale volcanic range (Danakil depression, Ethiopia), approximate scale 1:100.000. CNR-CNRS, Geotechnip.

Barberi, F., Cheminee, J.L., Varet, J., 1973. Long-lived lava lakes of Erta Ale volcano. Revue de Geographie Physique et de Geologie Dynamique 15, 347–352.

Barrat, J.A., Fourcade, S., Jahn, B.M., Cheminee, J.L., Capdevila, R., 1998. Isotope (Sr, Nd, Pb, O) and trace-element geochemistry of volcanics from the Erta Ale Range (Ethiopia). Journal of Volcanology and Geothermal Research 80, 85–100.

Bellier, O., Sebrier, M., 1994. Relationship between tectonism and volcanism along the Great Sumatran Fault Zone deduced by spot image analyses. Tectonophysics 233, 215–231.

Bosworth, W., Burke, K., Strecker, M., 2003. Effect of stress fields on magma chamber stability and the formation of collapse calderas. Tectonics 22, 1042, doi:10.1029/2002TC001369.

Cole, J.W., Milner, D.M., Spinks, K.D., 2005. Calderas and caldera structures: a review. Earth Science Reviews 69, 1–96.

Corti, G., Bovini, M., Conticelli, S., Innocenti, F., Manetti, P., Sokoutis, D., 2003. Analogue modelling of continental extension: A review focused on the relations between the patterns of deformation and the presence of magma. Earth Science Reviews 63, 169–247.

De Silva, S.L., 1989. Altiplano-Puna volcanic complex of the central Andes. Geology 17, 1102–1106.

Eagles, G., Gloaguen, R., Ebinger, C., 2002. Kinematics of the Danakil microplate. Earth and Planetary Science Letters 203, 607–620.

Gudmundsson, A., 1988. Formation of collapse calderas. Geology 16, 808–810.

Gudmundsson, A., 1992. Formation and growth of normal faults at the divergent plate boundary in Iceland. Terra Nova 4, 464–471.

Gudmundsson, A., 1998. Magma chambers modeled as cavities explain the formation of rift zone central volcanoes and their eruption and intrusion statistics. Journal of Geophysical Research 103, 7401–7412.

Gudmundsson, A., Loetveit, I.F., 2005. Dike emplacement in a layered and faulted rift zone. Journal of Volcanology and Geothermal Research 144, 311–327.

Harris, A.J.L., Flynn, L.P., Rothery, D.A., Oppenheimer, C., Sherman, S.B., 1999. Mass flux measurements at active lava lakes: implications for magma recycling. Journal of Geophysical Research 104, 7117–7136.

Harris, A.J.L., Carniel, R., Jones, J., 2005. Identification of variable convective regimes at Erta Ale lava lake. Journal of Volcanology and Geothermal Research 147, 207–223.

Hayward, N.J., Ebinger, C.J., 1996. Variations in the along-axis segmentation of the Afar Rift system. Tectonics 15, 244–257.

Holohan, E., Troll, V.R., Walter, T.R., Munn, S., McDonnell, S., Shipton, Z.K., 2005. Elliptical calderas in active tectonic settings: an experimental approach. Journal of Volcanology and Geothermal Research 144, 106–119.

Jestin, F., Huchon, P., Gaulier, J.M., 1994. The Somalia plate and the East African Rift System: present-day kinematics. Geophysical Journal International 116, 637–654.

Le Pichon, X., Francheteau, J., 1978. A plate tectonic analysis of the Red Sea-Gulf of Aden area. Tectonophysics 46, 369–406.

Lipman, P.W., 1997. Subsidence of ash-flow calderas: relation to caldera size and magma-chamber geometry. Bulletin of Volcanology 59, 198–218.

Manighetti, I., Tapponier, P., Gillot, P.Y., Jacques, E., Courtillot, V., Armijo, R., Ruegg, J.C., King, G., 1998. Propagation of rifting along the Arabia-Somalia plate boundary: into Afar. Journal of Geophysical Research 103, 4947–4974.

Manighetti, I., Tapponier, P., Courtillot, V., Gallet, Y., Jacques, E., Gillot, P.Y., 2001. Strain transfer between disconnected, propagating rifts in Afar. Journal of Geophysical Research 106, 13613–13665.

Marti, J., Ablay, G.J., Redshaw, L.T., Sparks, R.S.J., 1994. Experimental studies of collapse calderas. Journal of the Geological Society of London 151, 919–929.

Mauduit, T., Dauteuil, O., 1996. Small-scale models of oceanic transform zones. Journal of Geophysical Research 98, 12251–12265.

Mulugeta, G., 1985. Dynamic models of continental rift valley systems. Tectonophysics 113, 49–73.

McKenzie, D.P., Davies, D., Molnar, P., 1970. Plate tectonics of the Red Sea and East Africa. Nature 226, 243–248.

Minor, S.A., 1995. Superposed local and regional paleostresses: fault-slip analysis of Neogene extensional faulting near coeval caldera complexes, Yucca Flat, Nevada. Journal of Geophysical Research 100, 10507–10528.

Mohr, P.A., 1972. Surface structure and plate tectonics of Afar. Tectonophysics 15, 3–18.

Oppenheimer, C., Francis, P., 1998. Implications of longeval lava lakes for geomorphological and plutonic processes at Erta Ale volcano, Afar. Journal of Volcanology and Geothermal Research 80, 101–111.

Oppenheimer, C., McGonigle, A.J.S., Allard, P., Wooster, M.J., Tsanev, V., 2004. Sulfur, heat and magma budget of Erta Ale lava lake, Ethiopia. Geology 32, 509–512.

Ranalli, G., 1995. Rheology of the Earth. Chapman and Hall, London.

Roche, O., Druitt, T.H., Merle, O., 2000. Experimental study of caldera formation. Journal Geophysical Research 105, 395–416.

Rubin, A.M., Pollard, D.D., 1988. Dike-induced faulting in rift zones of Iceland and Afar. Geology 16, 413–417.

Tapponier, P., Armino, R., Manighetti, I., Courtillot, V., 1990. Bookshelf faulting and horizontal block rotations between overlapping rifts in southern Afar. Geophysical Research Letters 17, 1–4.

Tazieff, H., Varet, J., Barberi, F., Giglia, G., 1972. Tectonic significance of the Afar (or Danakil) depression. Nature 235, 144–147.

Tentler, T., 2003. Analogue models of tension fracture pattern in relation to mid-oceanic ridge propagation. Geophysical Research Letters 30, 1268, doi:10.1029/2002GL015741.

Turcotte, D.L., Schubert, G., 2002. Geodynamics, Second ed. John Wiley, New York, 452 pp.

Walker, G.P.L., 1990. Geology and Volcanology of the Hawaiian Islands; Review Article. Pacific Science 44, 315–347.

Walter, T.R., Troll, V.R., 2001. Formation of caldera periphery faults: an experimental study. Bulletin of Volcanology 63, 191–203.

Weijermars, R., 1986. Scaling of Newtonian and non-Newtonian fluid dynamics without inertia for quantitative modelling of rock flow due to gravity (including the concept of rheological similarity). Physics of the Earth and Planetary Interiors 43, 316–330.

Williams, H., 1941. Calderas and their origin. University of California Bulletins of the Department of Geological Science 21, 239–346.

Yoshida, T., 2001. The evolution of arc magmatism in the NE Honshu arc, Japan. Tohoku Geophysics Journal 36, 131–249.